SAND2007-3697C

MEASUREMENT OF THE DYNAMIC β–γ PHASE BOUNDARY IN TIN

Jean-Paul Davis and Dennis B. Hayes

Sandia National Laboratories,[*] Albuquerque, NM 87185-1181

Abstract: Experiments performed on the Z machine at Sandia Labs used magnetically generated planar ramp waves to quasi-isentropically compress pre-heated solid tin across the equilibrium β–γ phase boundary. Velocity history measurements at a tin/window interface exhibited features that could be consistently related, through simulations, to the β–γ structural transformation occurring in the bulk tin. The simulations used a homogeneous phase-mixture model with a γ-phase energy offset that was adjusted to match the measured velocity feature. This determined the phase-boundary pressure from experiment and the phase-boundary temperature from the β-phase equation of state. Due to wave interactions, measurements using sapphire windows were more difficult to interpret than those using LiF windows and thus led to results with larger uncertainty. Results did not display the hysteretic overshoot seen in static and shock experiments on other phase-transforming materials.

Keywords: tin, phase transition, phase boundary, isentropic compression
PACS: 61.66.Bi, 62.50.+p, 64.60.-i, 64.70.-p, 64.70.Kb

INTRODUCTION

An isentropic compression technique (ICE) has been developed at Sandia Labs using the fast pulsed-power Z accelerator to provide ramped magnetic-pressure loading of material samples [1]. Evolution of a ramped compression wave propagating through a material is sensitive to the derivative of the material's stress-strain response. The method is useful for studying structural phase transitions under dynamic compression, due to the rapid changes in wave speed upon entering or exiting a mixed-phase region. Phase boundaries can be measured for compression to peak pressures where shock loading would overdrive the transition. Dynamic phase boundaries can be mapped by pre-heating samples to different initial temperatures.

The β–γ phase boundary in tin (Sn) has a very steep dP/dT and occurs in easily accessible ranges of temperature and pressure. The crystal structure transitions with increasing pressure from 2-lattice body-centered tetragonal (bct) in the β-phase to regular bct in the γ-phase. The β–γ volume change of 3–5% is large enough to be easily detectable by time-resolved velocity measurements.

EXPERIMENTS

The present data come from eight shots on Z, spanning initial temperatures from ambient to melt. Most of the pre-heated experiments used an apparatus similar to that described in [2] for liquid-tin experiments. Resistive heaters transferred heat either directly to the outer annulus of 12-mm diameter tin samples mounted on sapphire insulator discs, or to the anode drive panel on which 6-mm diameter tin samples were mounted directly. To

[*] Sandia is a multi-program laboratory operated by Sandia Corporation, a Lockheed Martin Company, for the United States Department of Energy under Contract DE-AC04-94AL85000.

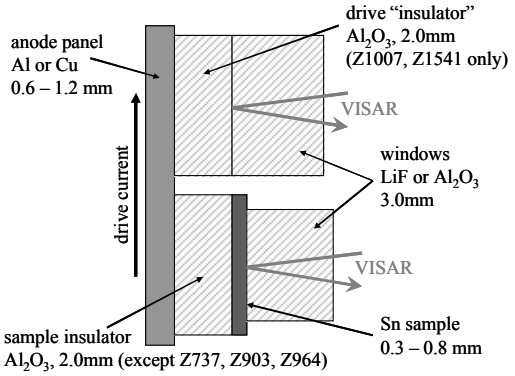

FIGURE 1. Schematic of the experimental configuration. The insulator layers exist only for certain shots as indicated; when not used, the two adjacent layers are bonded directly together. Al_2O_3 refers to z-cut sapphire.

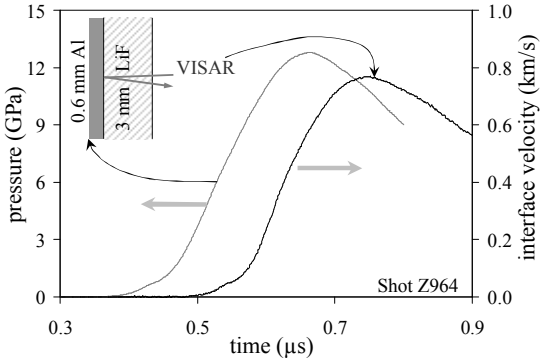

FIGURE 2. Example drive measurement from shot Z964; measured window-interface velocity history on right, effective stress loading history computed by backward integration on left.

measure temperature, fine-gauge thermocouples were bonded either into grooves in the insulator, or to the anode panel itself if there was no insulator.

Fig. 1 shows the experimental configuration for velocity interferometry (VISAR) measurements at both a tin sample and a separate sample-less location on the same anode. The latter allows estimation of the effective pressure history at the drive side of the anode by integrating the equations of motion backward in Lagrangian coordinate from the measurement position [3] (see Fig. 2). This pressure history is used to drive forward simulations that obviate magneto-hydro-dynamics considerations. Table 1 lists each sample considered, which include fine-grain (40-50 μm) and course-grain (300-1000 μm) polycrystalline tin, single-crystal <100> tin, and resolidified samples from liquid-tin experiments where a heater failed (these had non-uniform grain texture). Confidence in initial temperature T_0 is ±5 K except where noted.

Two of the measured velocity profiles are presented in Fig. 3. A ramp wave propagating through tin develops a kink at the phase boundary due to a sudden decrease in wave speed at the mixed-phase region. Wave interactions map this kink onto the interface velocity history, evident on both profiles in Fig. 3 about halfway to peak velocity. For a sapphire window, which has higher acoustic impedance than tin, interface pressure can cross the phase boundary prior to arrival of the kink feature from the bulk tin, complicating the wave interactions and making interpretation more difficult.

Z1541WB exhibits an unusually strong precursor, about 1.2 GPa in the tin. Seen in many of the single-crystal and resolidified tin data, this unexplained phenomenon may arise from localized gaps in bond layers due to thermal distortions. Another technical problem encountered was sample and bond thickness uncertainty due to deformation of the tin during assembly. These and other issues did not affect analysis, which relies solely on the velocity level of the kink in the measured profile.

ANALYSIS

Simulations of the experiments used a homogeneous mixture model for tin based on assumptions introduced by Horie and Duvall [4], with a numerical method developed by Andrews [5], extended to N phases by Hayes [6], and implemented in the WONDY code [7]. Each phase has its own equation of state (EOS), and the mixture's extensive properties are mass-averaged over all phases. Each EOS used a Birch isotherm with constant c_v and Γ/v, with parameters and reference states from the work of Mabire and Héreil [8]. We characterize the position of the β–γ phase boundary using the γ-phase reference energy $E_{\gamma\text{-}ref}$, nominally 93.4 kJ/kg for $P_{\gamma\text{-}ref}$ = 9.4 GPa and $T_{\gamma\text{-}ref}$ = 300 K ($E_{\beta\text{-}ref}$ = 0 kJ/kg). The model includes a one-parameter kinetics law, but this was set close to equilibrium. Strength was neglected. Other materials in the simulations (Al, Cu, Sapphire, LiF) used a Mie-

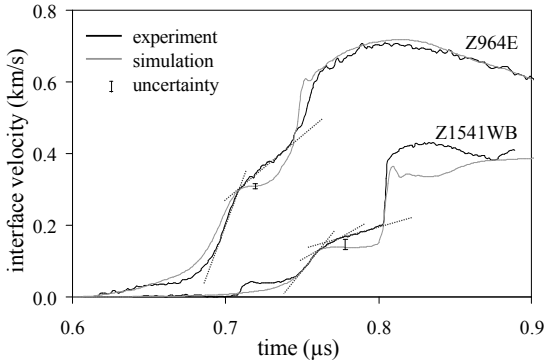

FIGURE 3. Window interface velocity measurements (black) from Z964E (LiF window) and Z1541WB (sapphire window); simulated velocity profiles with adjusted $E_{\gamma\text{-}ref}$ (gray). Dotted lines indicate kinks in measured velocity, vertical bars show uncertainty in matching kink.

Gruneisen EOS with linear U_s-U_p Hugoniots and no account taken of elevated temperature nor strength.

Each measurement was simulated using its effective drive pressure history and the nominal value of $E_{\gamma\text{-}ref}$. The resulting simulated interface velocity history exhibits a plateau feature due to the phase transition occurring in the bulk tin. If the velocity level of this plateau did not match that of the phase-transition kink in the experimental data, further simulations were performed with different values of $E_{\gamma\text{-}ref}$ until it did match. Examples of adjusted-$E_{\gamma\text{-}ref}$ simulations are shown in Fig. 3. The procedure is somewhat subjective, thus uncertainties were determined by considering the range of possible interpretations, and could be large for data with more than one kink (Z1541WB in Fig. 3) or no distinct kink. The experimental data generally do not exhibit a flat plateau region, probably due to metastability or kinetics effects. Only the velocity level need match; wave arrival time is unimportant.

Once the kink was matched by adjusting $E_{\gamma\text{-}ref}$, pressure and temperature on the phase boundary were extracted from the simulation by inspection of spatial distributions through the sample thickness taken at an appropriate time when the transition occurs near the drive side of the sample, as shown in Fig. 4. Pressure and temperature were read at the Lagrangian position where γ-phase mass fraction deviates from 0. In effect, this procedure obtains the phase-boundary pressure from the experimental measurement of a velocity kink at the interface, using the tin EOS to account for wave interactions.

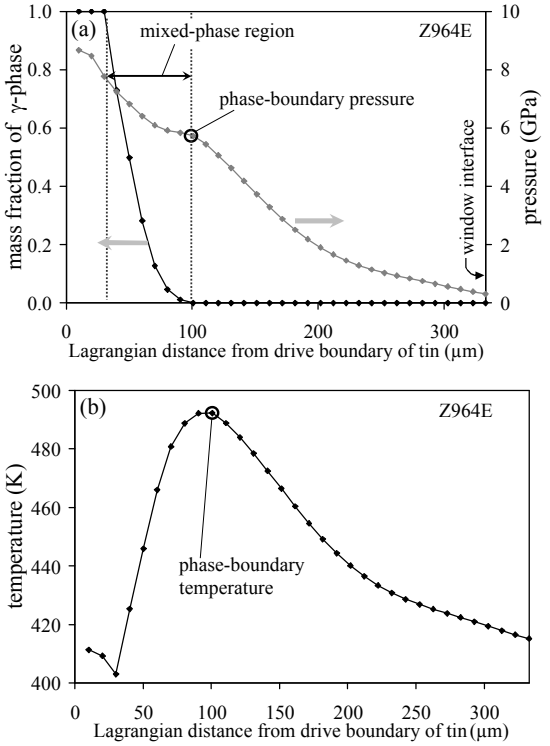

FIGURE 4. Snapshot of spatial distribution of (a) γ-phase mass fraction and pressure, and (b) temperature from adjusted-$E_{\gamma\text{-}ref}$ simulation for Z964E, showing determination of phase-boundary pressure and temperature.

The corresponding phase-boundary temperature then comes directly from the β-phase EOS.

RESULTS

Pressure and temperature on the β–γ phase boundary, determined as above for the 18 samples in Table 1, are plotted in Fig. 5 using filled and open circles according to window material. Short lines through each datum indicate uncertainty due to difficulties of interpretation. Uncertainty perpendicular to these lines is due to uncertainties in the initial temperature (quite small in most cases) and the rise in temperature of β-phase material along an isentrope (assumed to be well known). The present model equilibrium phase boundaries, static compression data [9,10], and data from shock/release experiments [8] are shown for comparison. Much of the data fall close to the equilibrium phase

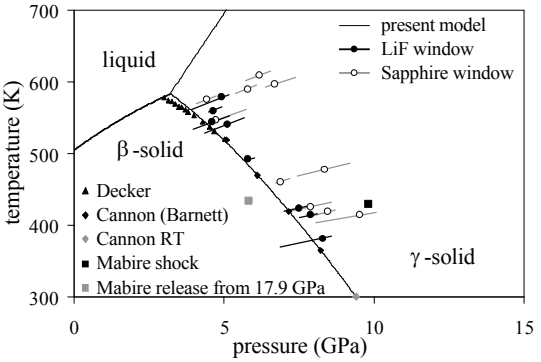

FIGURE 5. Phase diagram for tin: present model phase boundaries (——), static data [9,10] (▲, ♦, ♦), shock and release data [8] (■, ■), and present results (● for experiments with a LiF window, ○ for experiments with a Sapphire window) with uncertainty ranges.

boundary with considerably less hysteretic overshoot than seen under shock loading.

The six experiments falling furthest from the model phase boundary all used a sapphire window. Two of these were resolidified samples with large uncertainty in initial temperature, and could show better agreement if the actual temperature was much lower. Other data may suffer from as-yet unidentified experimental difficulties. Further work is needed to determine the effects of metastability and kinetics on interpretation of kinks in the measured window velocity profiles for LiF and sapphire windows on tin.

REFERENCES

1. Hall, C. A. et al, *Rev. Sci. Instrum.* **72**, 3587 (2001).
2. Davis, J.-P. and Foiles, S., *Experimental and Computational Study of the Liquid–Solid Transition in Tin*, Sandia National Laboratories Report SAND2005-6522, October 2005.
3. Hayes, D. B. et al, *J Appl. Phys.* **94**, 2331 (2003).
4. Horie, Y. and Duvall, G. E., *Behavior of Dense Media under High Dynamic Pressure*, IUTAM Symposium on High Dynamic Pressure, Gordon and Breach, New York, 1968, p. 355.
5. Andrews, D. J., *J. Comp. Phys.* **7**, 310 (1971).
6. Hayes, D. B., *J Appl. Phys.* **46**, 3438 (1975).
7. Kipp, M. E. and Lawrence, R. J., *WONDY V – A One-Dimensional Finite-Difference Wave Propagation Code*, Sandia National Laboratories Report SAND81-0930, June 1982.
8. Mabire, C. and Héreil, P. L., *J. Physique IV* **10**, Pr9/749 (2000).
9. Decker, D. L., Jorgensen, J. D., and Young, R. W., *High Temp.–High Pres.* **7**, 331 (1975).
10. Cannon, J. F., *J. Phys. Chem. Ref. Data* **3**, 781 (1974); Barnett, J. D., Bennion, R. B. and Hall, H. T., *Science*, **141**, 1041 (1963).

TABLE 1. Experimental details and nominal results, grouped by window material and sorted in order of increasing temperature; Al_2O_3 = z-cut sapphire, PC = polycrystalline, SC = single-crystal. Fine-grain tin samples were provided by G. T. Gray of Los Alamos National Laboratory. Parentheses indicate lack of precise measurement, and thus large uncertainty.

Experiment	Anode	Insulator	Tin Sample	Window	T_0 (K)	$E_{\gamma\text{-}ref}$ (kJ/kg)	P (GPa)	T (K)
Z737N	809 μm Al	—	302 μm PC-fine	LiF	300	94.5	8.29	381
Z1285WB	1212 μm Al	2005 μm Al_2O_3	505 μm SC <100>	LiF	330	95.3	7.88	414
Z1366WT	1006 μm Al	2004 μm Al_2O_3	354 μm SC <100>	LiF	340	94.5	7.50	423
Z964E	611 μm Al	—	333 μm PC-course	LiF	410	94.0	5.80	492
Z1541ET	754 μm Cu	(2000 μm) Al_2O_3	361 μm SC <100>	LiF	455	95.0	5.11	541
Z1541EB	759 μm Cu	(2000 μm) Al_2O_3	540 μm SC <100>	LiF	463	94.0	4.60	544
Z1366SB	1013 μm Al	2019 μm Al_2O_3	502 μm SC <100>	LiF	480	95.0	4.63	560
Z1366ST	1006 μm Al	2004 μm Al_2O_3	504 μm SC <100>	LiF	492	96.7	4.93	579
Z1285EB	1211 μm Al	2004 μm Al_2O_3	496 μm SC <100>	Al_2O_3	320	100.0	9.52	414
Z903ET2	615 μm Al	—	345 μm PC-course	Al_2O_3	(325)	97.0	8.45	419
Z1366EB	1013 μm Al	1999 μm Al_2O_3	504 μm SC <100>	Al_2O_3	339	96.0	7.88	426
Z1080ET	613 μm Cu	2002 μm Al_2O_3	810 μm SC <100>	Al_2O_3	375	95.0	6.88	461
Z1285NT	1212 μm Al	1998 μm Al_2O_3	353 μm SC <100>	Al_2O_3	377	100.0	8.36	478
Z1541WB	760 μm Cu	(2000 μm) Al_2O_3	514 μm SC <100>	Al_2O_3	467	94.5	4.73	547
Z1007SB	810 μm Al	2189 μm Al_2O_3	696 μm resolidified	Al_2O_3	(485)	102.0	6.68	597
Z1366NT	1011 μm Al	2011 μm Al_2O_3	501 μm SC <100>	Al_2O_3	490	99.5	5.80	590
Z1541NB	747 μm Cu	1869 μm Al_2O_3	508 μm resolidified	Al_2O_3	(495)	95.5	4.42	576
Z1541SB	756 μm Cu	1879 μm Al_2O_3	509 μm resolidified	Al_2O_3	(500)	101.5	6.18	609